Published in
Thin-Walled Structures 135 (2019) 446-452
https://doi.org/10.1016/j.tws.2018.11.012
Received 19 July 2018; Received in revised form 10 October 2018; Accepted 13 November 2018

An analytical solution of distortional buckling resistance of cold-formed steel channel-section beams with web openings

Nan-ting Yu[a,b], Boksun Kim[b], Wei-bin Yuan[a,c*], Long-yuan Li[b], Feng Yu[a]

(a) College of Architecture and Civil Engineering, Zhejiang University of Technology, Hangzhou 310023, PR China

(b) School of Engineering, University of Plymouth, Plymouth PL4 8AA, UK

(c) Key Laboratory of Civil Engineering Structure & Disaster Prevention and Mitigation Technology of Zhejiang Province, Hangzhou 310023, PR China

Abstract - Circular holes can be commonly found in the web of cold-formed steel beams to accommodate services such as electric wires and pipelines. The presence of holes will reduce the critical buckling stress of the beams. Hancock proposed solution for determining the distortional critical stress of channel section beams, but limited to the sections without holes. This paper presents an analytical study on the distortional buckling of cold-formed steel channel-section beams with circular holes in the web. Hancock's solution has been modified to derive a simple formulation for approximating the elastic critical stress and moment of distortional buckling of the channel-section beams with circular holes in the web, which are compared with those from the finite element buckling analysis using ANSYS. Finally, the influence of multiple holes on the distortional buckling behaviour and corresponding elastic buckling stress of beams in bending is discussed.

Keywords: Cold-formed steel; Channel section; Distortional buckling; Circular openings; Analytical solution; Finite element analysis

1. Introduction

Thin-walled, perforated cold-formed steel (PCFS) structural components are widely used in construction industry. For example, in low-rise building construction, openings can be found in the web of cold-formed steel beams to allow access for electric wires and pipes; in storage rack structures upright members have many perforations along the length to allow for variable heights of the shelf. The presence of holes may lead to the decrease in cross-section and buckling resistance of the members [1]. Similar to cold-formed steel (CFS) members, PCFS members may experience three typical buckling modes: local, distortional and global buckling when they are subject to compression or bending.

However, because of various parameters including perforations shape, size and location, it is difficult to determine the critical buckling stresses of PCFS sections directly [2].

Early researchers focussed on the buckling and post-buckling response of perforated plates [3-12]. Miller and Pekoz [4] used the unstiffened strip approach to predict the post-buckling strength of plates with holes, the theoretical results were compared with the stud column tests. Shanmugam et al. [5] evaluated the ultimate load of perforated plates with different boundary conditions by using finite element method. Moen and Schafer [6] put forward some expressions to approximate the influence of web holes on the critical buckling stress of perforated plates under compression or bending. The finite element parametric studies showed that holes may decrease or increase the critical buckling stress, depending on the hole geometry and spacing. The elastic buckling behaviour of plates with circular and rectangular holes under compression and bending loads was explored by Maiorana et al. [7]. Paik [8] conducted a series of nonlinear finite element analysis (FEA) and presented a closed-form empirical formula for predicting the ultimate compressive strength of steel plates with a single circular hole. Later, Paik and his colleagues [9] undertook the experimental and numerical investigations on the buckling and ultimate strength of plates and stiffened panels with an opening subjected to axial compression. The experimental database they collected was very useful for the future design guide. Ge et al. [10] performed 954 linear and non-linear finite element analyses for the plates with openings, including the relative parametric studies. The stability of a perforated square plate subjected to biaxial load was investigated by El-Sawy [11]. Kumar et al. [12] presented interaction equations based on non-linear regression analysis for determining the ultimate strength of stiffened panels with circular opening under axial and lateral loads.

Simplified methods for approximating local, distortional and global elastic critical buckling loads of PCFS columns and beams were developed by Moen and Schafer [2]. Kulatunga and Macdonald [13] conducted a finite element analysis using ANSYS for PCFS columns, and the corresponding accuracy of the results was verified by using experimental and theoretical results. It is showed that the perforations can influence the ultimate load of PCFS columns under compression. Crisan et al. [14-15] studied the behaviour of PFCS sections in compression using experimental, numerical and theoretical methods. Experiments were carried out by Moen and Schafer [16] to observe the relationship between elastic buckling and tested response of PCFS columns. Compression tests were conducted on 24 short and intermediate length CFS columns with and without holes. The results showed that slotted holes might modify the local and distortional elastic buckling half-wavelengths and change the critical elastic buckling loads. Yuan et al. [17] presented an analytical formulation to predict the distortional critical buckling stress of PCFS beams, the distortional buckling model of CFS sections recommended in EN1993-1-3 was employed. However, the distortional buckling stress obtained from modified EN1993-1-3 [18] model was found to be conservative, compared with that from Hancock [19] method or numerical methods.

Finite strip method was widely used as a method to determine the elastic critical stress of CFS sections, but it is hard to deal with perforated members. Sputo and Tovar [20], Tovar and Sputo [21] used finite strip method to determine the elastic longwave, distortional and local buckling stress of PCFS studs, in which several different models were chosen to represent the effect of web openings. Smith and Moen [22] utilised approximate finite strip calculation methods to predict the critical elastic local, distortional and global load of a PCFS column. The reduction of the bending stiffness of the web was taken into account with the reduced thickness in the finite strip analysis.

Recent studies have been proposed to extend the direct strength method to determine the ultimate strength of PCFS sections [22]. Moen and Schafer [23] derived design expressions to extend direct strength method to PCFS columns, which were validated by existing experiments and finite-element simulations. Wang and Young [24] investigated the flexural behaviour of PCFS built-up beams including the failure modes and ultimate moment capacities by using experimental method. A total of 43 beams with 10 section sizes and different hole diameters were tested. The current direct strength method was extended for PCFS beams. Yao and Rasmussen [25-26] developed an inelastic material and geometric nonlinear isoparametric spline finite strip method for PCFS structures. Later, they investigated the inelastic local buckling behaviour of PCFS columns and perforated simply supported plates under compression loads [27].

In this paper, a simple analytical formulation according to the distortional buckling model presented by Hancock is proposed to determine the elastic critical buckling stress and moment of distortional buckling of PCFS channel-section beams with circular holes in web. The proposed method is verified by using finite element buckling analysis. The influence of perforations on the elastic critical stress and moment of distortional buckling is evaluated.

2. An analytical study for determining distortional buckling moment

The geometry of PCFS channel-section beam is shown in Fig. 1. It is supposed that the circular holes are centered along the neutral axis of the web evenly. The diameter of the hole is d. For the convenience of further investigation, the beam length is regarded as $L=n\pi d/2$, where n represents the quantities of holes in the web. This means that the opening area is equal to the solid area in the opening web strip. In this work, the PCFS channel-section beam is assumed to be simply supported at its two ends and subject to bending about the major axis.

It is known that the distortional buckling may occur in open cross sections and its half-wavelength is several times larger than the dimension of the cross-section. Distortional buckling of CFS members is usually identified by the rotation and translation of the corners of the cross-section [28-30]. For flexural members, only the compression flange and lip rotate around the flange-web junction; the web may undergo out-of-plane flexural at the same half-wavelength when the flange-lip element buckles. In Hancock's model [19][28], the lateral spring and rotational spring represent the influence of web on the

flange and lip system, the position of the springs is at the flange-web junction (see Fig. 2a). The value of the lateral spring stiffness k_x is assumed to be zero. The critical buckling stress of the flange and lip system can be expressed as follows [19],

$$\sigma_{cr} = \frac{E}{2A}\left\{(\alpha_1 + \alpha_2) - \sqrt{[(\alpha_1 + \alpha_2)^2 - 4\alpha_3]}\right\} \quad (1)$$

in which

$$\alpha_1 = \frac{\pi^2 A}{\lambda^2\left(A{x_c}^2 + I_x + I_y\right)}(I_x b^2 + 0.039J\lambda^2) + \frac{A\lambda^2 k_\phi}{\pi^2 E(A{x_c}^2 + I_x + I_y)}$$

$$\alpha_2 = \frac{\pi^2}{\lambda^2}\left(I_y + \frac{2A}{A{x_c}^2 + I_x + I_y} y_c b I_{xy}\right)$$

$$\alpha_3 = \frac{\pi^2}{\lambda^2}\left(\alpha_1 I_y - \frac{\pi^2 A}{\lambda^2\left(A{x_c}^2 + I_x + I_y\right)} {I_{xy}}^2 b^2\right)$$

$$\lambda = 4.8\left(\frac{I_x b^2 h}{2t^3}\right)^{0.25}$$

where σ_{cr} is the compressive stress at the compressive flange, E is the modulus of elasticity, A is the area of the flange and lip system, x_c and y_c are the distance from flange-web junction to the Y and X axes respectively, the original point is at the centroid of the flange and lip system, I_x and I_y are the second moment of the section area about the x and y axes, I_{xy} is the product moment of the section area, J is the torsion constant and λ is the buckling half-wavelength.

The value of the rotational spring stiffness k_Φ can be calculated as

$$k_\phi = \frac{4D}{h + 0.06\lambda}\left(1 - \frac{\sigma_{cr0}}{\sigma_w}\frac{h}{h + 2y_c}\right) \quad (2)$$

where σ_{cr0} is the buckling stress obtained by Eq.(1) when k_Φ is zero, σ_w is the buckling stress of web plate subject to the pure bending, $D=Et^3/12(1-\nu^2)$ is the bending rigidity of web strip without openings and ν is the Poisson's ratio.

In this present study, the circular holes are only displayed in the web so that the model presented by Hancock [19], in 1997 can be applied. However, in order to consider the effect of web openings, the rotational spring stiffness needs to be modified. It is assumed that the bending rigidity of the web strip where the holes are located is different from that of other parts where there is no holes. By applying the unit bending moment at the flange-web junction where the rotation spring is located, the rotational angle of loading point can be obtained, as shown in Fig. 2b. The strain energy of the web can then be expressed as follows,

$$U = \frac{1}{2D}\int_0^h \left(\frac{M}{h}x\right)^2 dx + \left(\frac{1}{2D_d} - \frac{1}{2D}\right)\int_{\frac{h-d}{2}}^{\frac{h+d}{2}} \left(\frac{M}{h}x\right)^2 dx \quad (0 \le x \le h) \quad (3)$$

The rotation of the web is

$$\varphi = \frac{\partial U}{\partial M} \tag{4}$$

The rotational spring stiffness can be obtained from Eq.(3) and Eq.(4) as follows,

$$k_{\phi}^{*} = \frac{3D}{h} \frac{1}{1 + (\frac{D}{D_d} - 1)\left(\frac{d}{h}\right)\left[\frac{3}{4} + \frac{1}{4}\left(\frac{d}{h}\right)^2\right]} \tag{5}$$

where $D_d = \alpha Et^3/12(1-\nu^2)$ is the bending rigidity of web strip with openings, α is an arbitrary constant defining the reduction of web bending rigidity. Since the holes are only located in the mid-strip, α can represent the effect of openings on the bending rigidity of the mid-strip. If α=1 then k_Φ=3D/h which represents the rotational spring stiffness with no holes in the web. In this case, α is set as 0.5, which represents the approach of equal width. The second term in Eq.(3) can be regarded as the reduction factor of the rotational spring stiffness β ,

$$\beta = \frac{1}{1 + (\frac{D}{D_d} - 1)\left(\frac{d}{h}\right)\left[\frac{3}{4} + \frac{1}{4}\left(\frac{d}{h}\right)^2\right]} \tag{6}$$

Further, the perforated web plates may buckle due to the plate buckling taken no account of the holes or the buckling of unstiffened strip (the web strip with one free edge) adjacent to the holes or the combination of the two [6]. Moen [31] developed an approach to predict the unstiffened strip buckling stress of web plates with holes, which accounts for the gradient of compression stress and the aspect ratio of the unstiffened strip. The hole size cannot be too large or small and the hole space cannot be too close. For the web plate with small holes, the holes may affect the half-wave length. Moreover, for the web plate with large holes, the unstiffened strips become narrow to increase its stiffness. When the hole space is close, buckling might be restrained at the holes. Hence, it is hard to develop an expression to predict the bucking stress of perforated web plates for various hole sizes and space. Nevertheless, the variation of the buckling stress of perforated web plates has minimal impact on the reduction factor in the bracket in Eq.(2). The rotational spring stiffness $k_{\Phi,d}$ of PCFS channel-section beams with circular holes in the web can be modified as,

$$k_{\phi,d} = \frac{2\beta Et^3}{5.46(h + 0.06\lambda)}\left[1 - \frac{1.11\sigma_{cr0}}{Et^2}\left(\frac{h^4\lambda^2}{12.56\lambda^4 + 2.192h^4 + 13.39\lambda^2h^2}\right)\right] \tag{7}$$

Substituting Eq.(7) into (1), the corresponding distortional buckling stress for pure bending can be obtained. The critical moment of distortional buckling is calculated as follows,

$$M_{cr} = \frac{2\sigma_{cr} I_{re}}{h} \tag{8}$$

where M_{cr} is the distortional buckling moment of PCFS channel-section beams and I_{re} is the second moment of the reduced area of channel section with holes in the web which can be expressed as follows,

$$I_{re} = I - \frac{td^3}{12} = 2\left(\frac{bt^3}{12} + \frac{bth^3}{4}\right) + \frac{th^3}{12} - \frac{td^3}{12} \quad (9)$$

where I is the second moment of the full area of channel section without holes in the web.

3. Finite element analysis

The elastic buckling loads of CFS beams without holes can be obtained from the elastic buckling curve using finite strip method (FSM). FSM can be performed more efficiently by using program CUFSM [32]. However, the problem is that the holes cannot be easily modelled with FSM, and therefore, to determine the buckling stress of PCFS beams the FEA is applied. In order to gain the lowest eigen-value, which represents the critical stress of distortional buckling, the size of channel sections should be carefully selected. Table 1 shows the cross-sectional dimensions and lengths of three chosen sections. Fig.3 shows the buckling curves of the three chosen channel sections without holes generated from CUFSM, where M_{cr} is the critical moment of the beam under pure bending and M_y is the yielding moment. It can be found that the lowest critical moments of local buckling of these three sections are higher than those of distortional buckling. When the range of beam length from 200 mm to 1350 mm (Section 1), from 300 mm to 1850 mm (Section 2) and from 400 mm to 1600 mm (Section 3), the minimum value is the distortional critical buckling stress of CFS channel-section beams.

The linear finite element analysis of PCFS beams is conducted by using the commercial software, ANSYS to explore the effects of holes on the distortional loads and failure modes shapes. The three sections in Table 1 were modelled. Each section employed four different sizes, whose hole diameter to web depth ratio, d/h ranged from 0.29 to 0.5. The beam length followed the formula of $L=n\pi d/2$. Two ends of the beam are simply supported and hence in the longitudinal axial direction the ends of the section are free to move but in the lateral and transverse directions are prevented from deforming. The displacement boundary conditions were applied to the lines at the two edges. The lateral displacement, the transverse displacement and the rotational displacement about the longitudinal axis are assumed to be zero. One node locates at the web at one of the ends is assumed to have zero axial displacement in order to avoid the rigid displacement in the longitudinal axial direction. The material properties of the beams are considered as typical cold-formed steel with modulus of elasticity E=205 GPa, Poisson's ratio ν=0.3 and yield stress f_y=390 MPa. The comparison of the critical buckling moment of CFS channel-section beams between FSM and FEA is shown in Fig.4. For the case of beams without holes, the difference of the results produced from FEA and FSM is less than 5%, which confirms the FEA shell-element model employed in the present study has good accuracy. Fig.5 shows a typical finite element mesh of a PCFS channel-section beam with circular holes in the web. The element sizes are set to 5 mm to ensure the accuracy of the results. Shell 181 in ANSYS was chosen for the finite element model. To simulate the pure moment, the uniform forces were applied on the flange lines, the linearly varied forces are applied on the web lines and lip lines, as shown in Fig.5.

The typical distortional buckling curves of PCFS channel-section beams with the four different sizes of circular holes can be found in Fig.6, where M_{cr} is the distortional buckling moment of PCFS channel-section beams, M_y is the yield moment of CFS beams without holes in the web. It can be observed from the figure that the curves have the similar tendency, the distortional buckling moment varies slightly around the minimum point because of the variation of beam length. It can also be seen that the critical moment is decreased while the holes become larger, this is because the restriction of the flange and lip system from web is weaker. In addition, the half wavelength of the beam also increases with the hole size. This implies that the holes might affect the half wavelength of distortional buckling modes.

Fig.7 shows the typical distortional buckling modes of PCFS channel-section beams obtained from the finite element analysis. It is shown that Sections 1 and 2 have three distortional buckling modes with one, two and three buckling waves, Section 3 has two distortional modes with one, two buckling waves in different beam lengths respectively. It can be seen from the figure that the distortional buckling of PCFS channel-section beams are characterised by the rotation of the flange and lip system around the flange-web junction. Fig.8 shows the comparison of buckling curves of PCFS channel-section beams obtained from the proposed analytical solution, and those from the finite element analysis for the four different values of d/h ratios. It can be observed from the figure that, the critical moment calculated from the proposed analytical solution has a very good agreement with those obtained from the finite element analysis. While, the critical moment calculated from the modified EN-1993-1-3 model [18] is slightly lower than the FEA data and hence is conservative. This is because EN-1993-1-3 model is based on the stiffened element buckled on the elastic foundation, the lip and half flange adjacent to the lip represent the distortional buckling behaviour. Its expression is simpler but the critical stress is inaccurate compared with that from the proposed approximate method. Eq.(1) and Eq.(8) give simple expressions to calculate the critical stress and moment of distortional buckling of PCFS channel-section beams with circular holes in the web.

4. Conclusions

This paper has presented an analytical study for calculating the distortional buckling moment of PCFS channel-section beams with circular holes in the web subjected to pure moment. The analytical solution is based on the Hancock's model, which is modified to include the effect of the presence of holes on the web. The results from the analytical study have been compared with those from the finite element analysis using ANSYS. The influence of holes on the distortional buckling behaviour has also been examined. From the present work, the following conclusions can be drawn:

- The flange and lip system model presented by Hancock can be used to calculate the critical stress of distortional buckling of PCFS channel-section beams if the rotational spring stiffness k_Φ is adequately reduced.

- The proposed analytical solution predicts the distortional buckling stress of PCFS channel-section beams, which is more accurate than that obtained from modified EN1993-1-3 model [17].
- The concept of equivalent width can be taken into account when determining the reduction factor of web bending rigidity.
- The distortional buckling moment of PCFS channel-section beams decreases as the hole size increases, but the half wave-length increases with the increase of hole size.

Acknowledgement

The first author would like to acknowledge the financial support received from the Chinese Scholarship Council for his PhD study at the University of Plymouth in the United Kingdom.

Reference

[1] Pham C.H. (2017). "Shear buckling of plates and thin-walled channel sections with holes." Journal of Constructional Steel Research, 128: 800-811.

[2] Moen C.D. and Schafer B.W. (2009). "Elastic buckling of cold-formed steel columns and beams with holes." Engineering Structures, 31(12): 2812-2824.

[3] Christoper J.B., Alan L.Y. and Mark B. (1987). "Stability of Plates with Rectangular Holes." Journal of Structural Engineering, 113(5): 1111-1116.

[4] Miller T.H. and Pekoz T. (1994). "Unstiffened Strip Approach for Perforated Wall Studs." Journal of Structural Engineering, 120: 410-421.

[5] Shanmugam N.E., Thevendran V. and Tan Y.H. (1999). "Design formula for axially compressed perforated plates." Thin-Walled Structures, 34: 1-20.

[6] Moen C.D. and Schafer B.W. (2009). "Elastic buckling of thin plates with holes in compression or bending." Thin-Walled Structures, 47(12): 1597-1607.

[7] Maiorana E., Carlo P. and Claudio M. (2009). "Elastic stability of plates with circular and rectangular holes subjected to axial compression and bending moment." Thin-Walled Structures, 47(3): 241-255.

[8] Paik J.K. (2007). "Ultimate strength of steel plates with a single circular hole under axial compressive loading along short edges." Ships and Offshore Structures, 2(4): 355-360.

[9] Kim U.N., Choe I.H. and Paik J.K. (2009). " Buckling and ultimate strength of perforated plate panels subjected to axial compression: experimental and numerical investigations with design formulations." Ships and Offshore Structures, 4(4): 337-361.

[10] Wang G., Sun H.H., Peng H. and Uemori R. (2009). "Buckling and ultimate strength of plates with openings." Ships and Offshore Structures, 4(1): 43-53.

[11] El-Sawy K.M. and Martini M.I. (2010). "Stability of biaxially loaded square plates with single central holes." Ships and Offshore Structures, 5(4): 283-293.

[12] Kumar M.S., Alagusundaramoorthy P. and Sundaravadivelu R. (2009). "Interaction curves for stiffened panel with circular opening under axial and lateral loads." Ships and Offshore Structures, 4(2): 133-143.

[13] Kulatunga M.P. and Macdonald M. (2013). "Investigation of cold-formed steel structural members with perforations of different arrangements subjected to compression loading." Thin-Walled Structures, 67: 78-87.

[14] Crisan A., Ungureanu V. and Dubina D. (2012). "Behaviour of cold-formed steel perforated sections in compression. Part 1—Experimental investigations." Thin-Walled Structures, 61: 86-96.

[15] Crisan A., Ungureanu V. and Dubina D. (2012). "Behaviour of cold-formed steel perforated sections in compression: Part 2—numerical investigations and design considerations." Thin-Walled Structures, 61: 97-105.

[16] Moen C.D. and Schafer B.W. (2008). "Experiments on cold-formed steel columns with holes." Thin-Walled Structures, 46(10): 1164-1182.

[17] Yuan W.B., Yu N.T. and Li L.Y. (2017). "Distortional buckling of perforated cold-formed steel channel-section beams with circular holes in web." International Journal of Mechanical Sciences, 126: 255-260.

[18] EN1993-1-3. Eurocode 3 - Design of steel structures – Part 1-3: General rules – Supplementary rules for cold-formed members and sheeting, BSI; 2006.

[19] Hancock G.J. (1997). "Design for distortional buckling of flexural members." Thin-Walled Structures, 27(1): 3-12.

[20] Sputo T. and Tovar J. (2005). "Application of direct strength method to axially loaded perforated cold-formed steel studs: Longwave buckling." Thin-Walled Structures, 43(12): 1852-1881.

[21] Tovar J. and Sputo T. (2005). "Application of direct strength method to axially loaded perforated cold-formed steel studs: Distortional and local buckling." Thin-Walled Structures, 43(12): 1882-1912.

[22] Smith F.H. and Moen C.D. (2014). "Finite strip elastic buckling solutions for thin-walled metal columns with perforation patterns." Thin-Walled Structures, 79: 187-201.

[23] Moen C.D. and Schafer B.W. (2011). "Direct strength method for design of cold-formed steel columns with holes." Journal of Structural Engineering, 137(5): 559-570.

[24] Wang L.P. and Young B. (2015). "Beam tests of cold-formed steel built-up sections with web perforations." Journal of Constructional Steel Research, 115: 18-33.

[25] Yao Z. and Rasmussen K.J.R. (2011). "Material and geometric nonlinear isoparametric spline finite strip analysis of perforated thin-walled steel structures—Analytical developments." Thin-Walled Structures, 49(11): 1359-1373.

[26] Yao Z. and Rasmussen K.J.R. (2011). "Material and geometric nonlinear isoparametric spline finite strip analysis of perforated thin-walled steel structures—Numerical investigations." Thin-Walled Structures, 49(11): 1374-1391.

[27] Yan Z. and Rasmussen K.J.R. (2012). "Inelastic local buckling behaviour of perforated plates and sections under compression." Thin-Walled Structures, 61: 49-70.

[28] Lau S.C.W. and Hancock G.J. (1987). "Distortional buckling formulas for channel columns." Journal of Structural Engineering, 113(5): 1063-1078.

[29] Li, L.Y. and Chen J.K. (2008). "An analytical model for analysing distortional buckling of cold-formed steel sections." Thin-Walled Structures, 46(12): 1430-1436.

[30] Zhu J. and Li L.Y. (2016). "A stiffened plate buckling model for calculating critical stress of distortional buckling of CFS beams." International Journal of Mechanical Sciences, 115-116: 457-464.

[31] Moen C.D. (2008) "Direct strength design for cold-formed steel members with perforations." Ph.D. Thesis, Johns Hopkins University.

[32] Schafer B.W. and Adany S. (2006). "Buckling analysis of cold-formed steel members using CUFSM: conventional and constrained finite strip methods." In: 18th International Specialty Conference on Cold-Formed Steel Structures, Orlando, Florida, October.

Table 1 Dimensions of CFS channel-sections (unit: mm)

Sections	Web depth, h	Flange width, b	Lip length, c	Thickness, t
Section 1	150	50	15	2
Section 2	200	70	20	2.5
Section 3	250	80	25	3

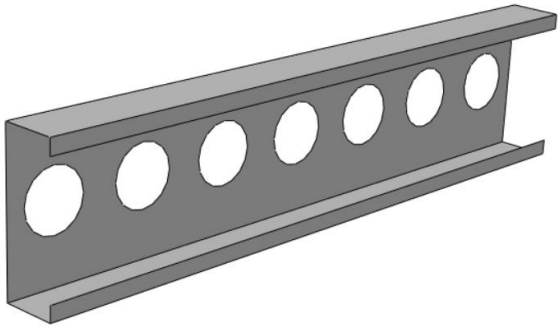

(a) in 3D

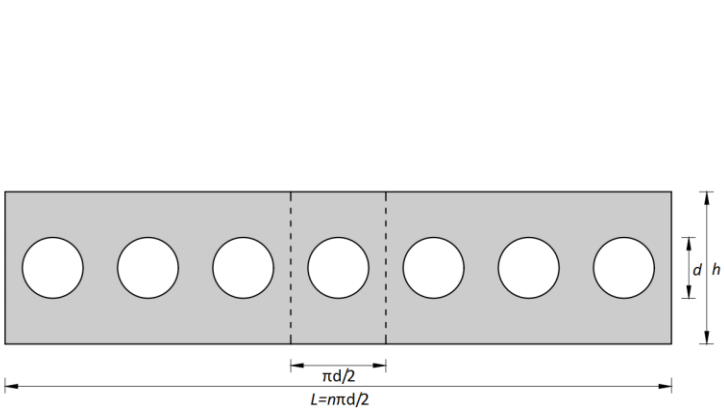

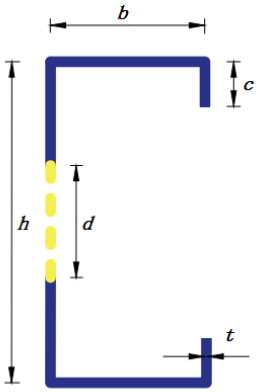

(b) web (c) cross-section

Fig. 1. PCFS channel-section beam geometry

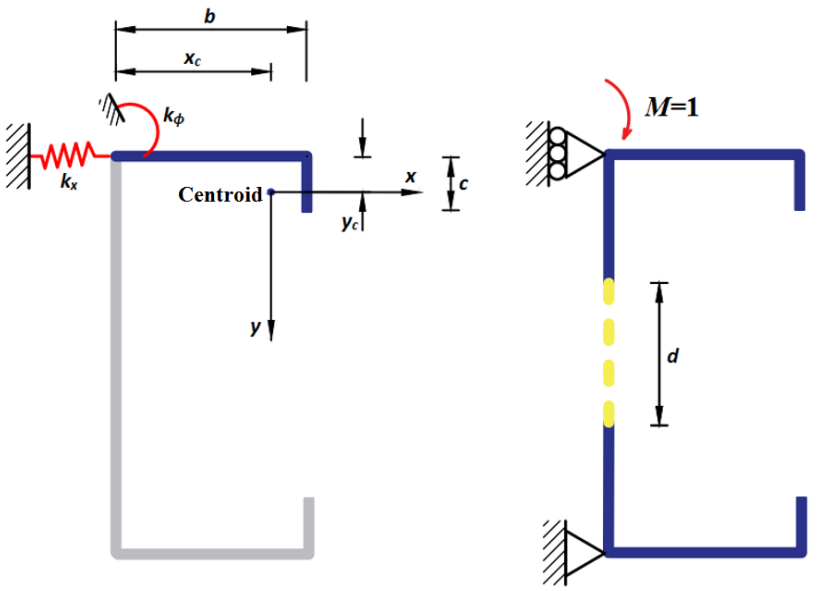

(a) (b)

Fig. 2. (a) Hancock distortional buckling model. (b) Model used to determine rotation spring stiffness

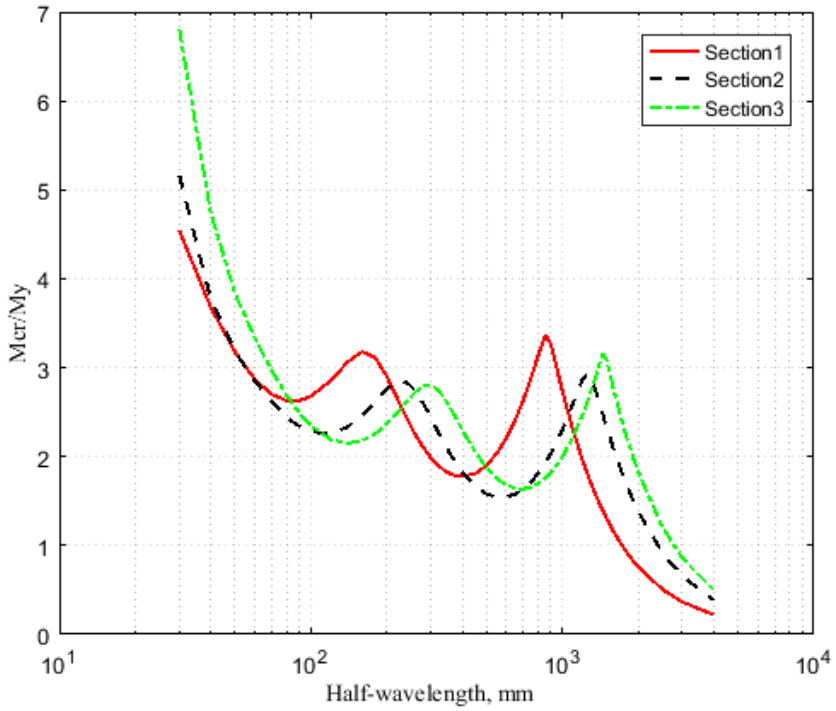

Fig. 3. Distortional buckling curves of CFS channel-section beams (σ_y=390 MPa, M_y is the yield moment)

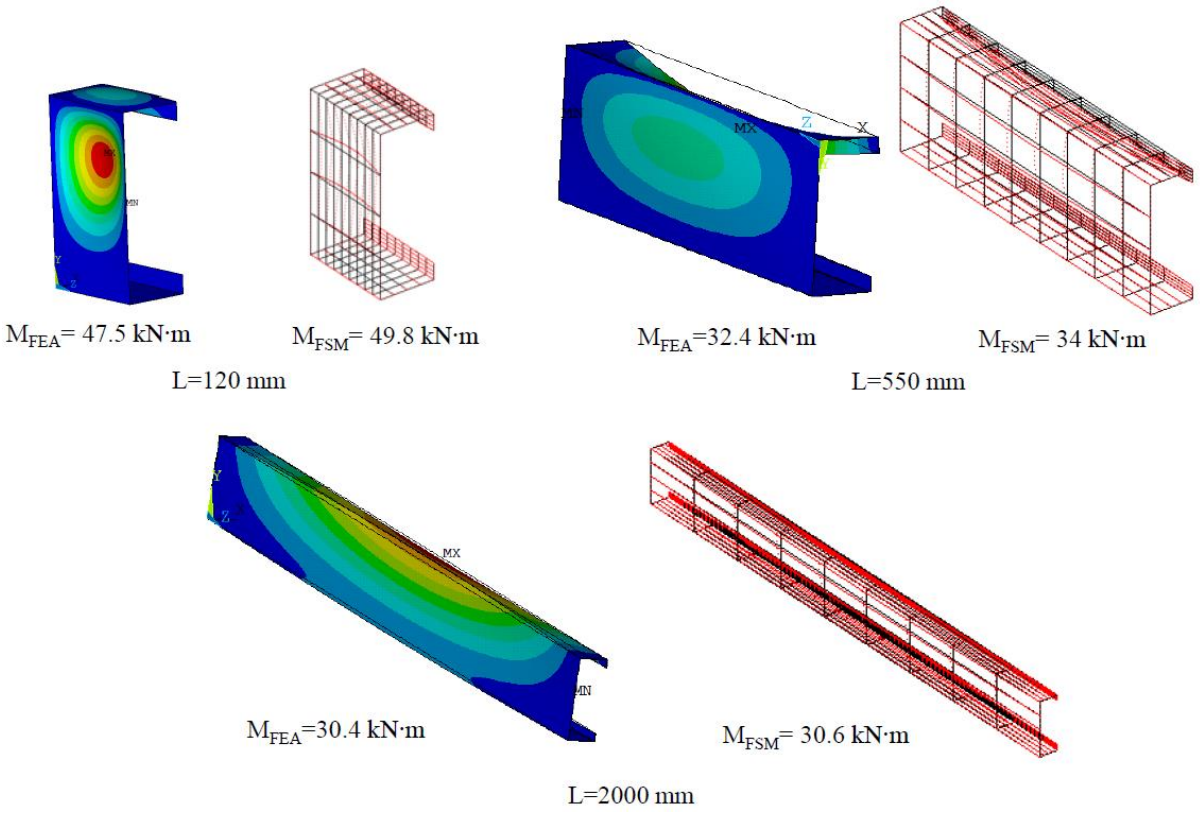

Fig. 4. Comparison of the critical buckling moment of CFS channel-section beams (M_{FSM} is the critical moment from FSM, M_{FEA} is the critical moment from FEA)

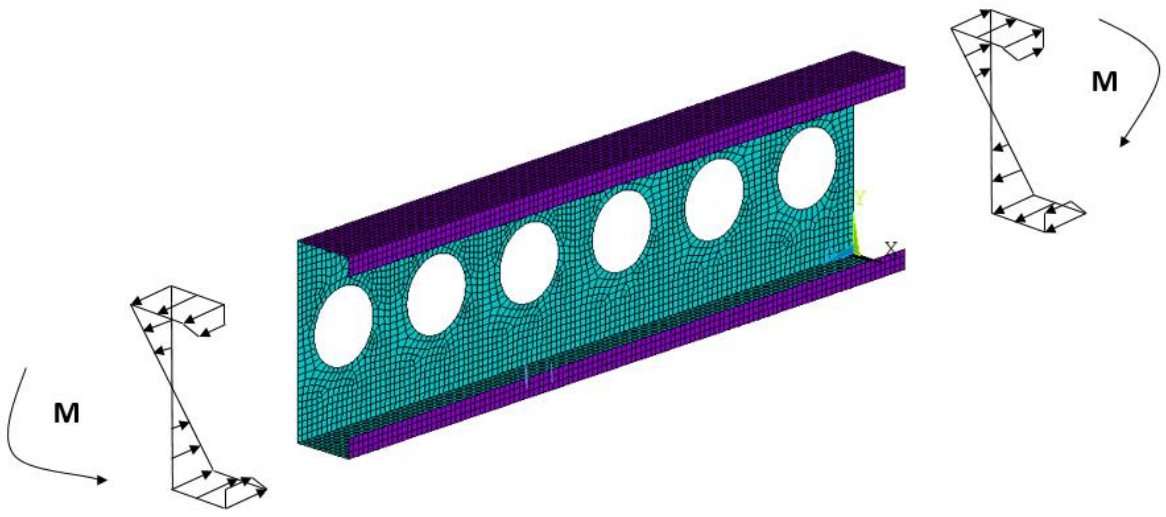

Fig. 5. Typical finite element mesh of a PCFS channel-section beam

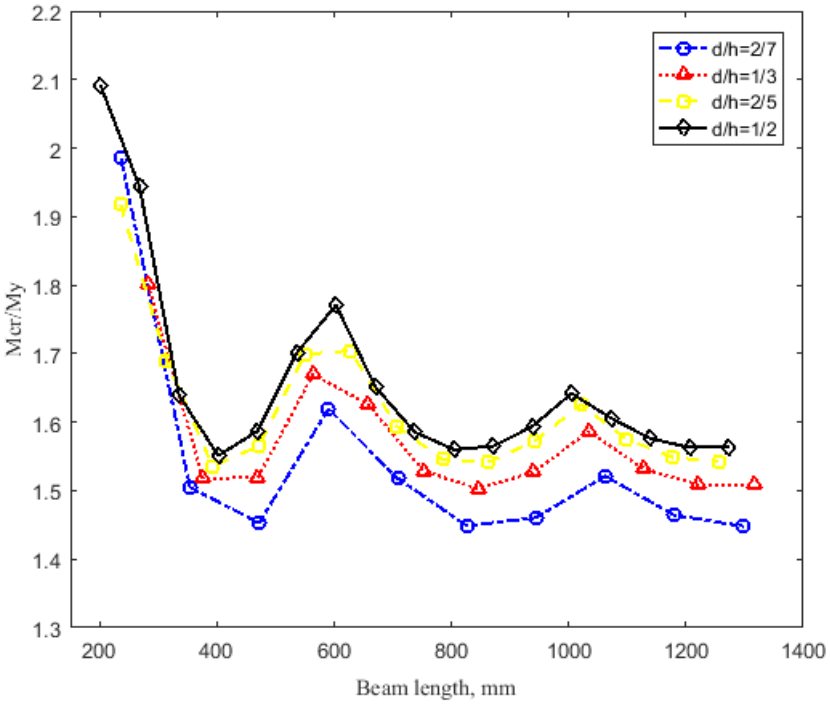

(a) Section 1 (h=150 mm, b=50 mm, c=15 mm, t=2 mm)

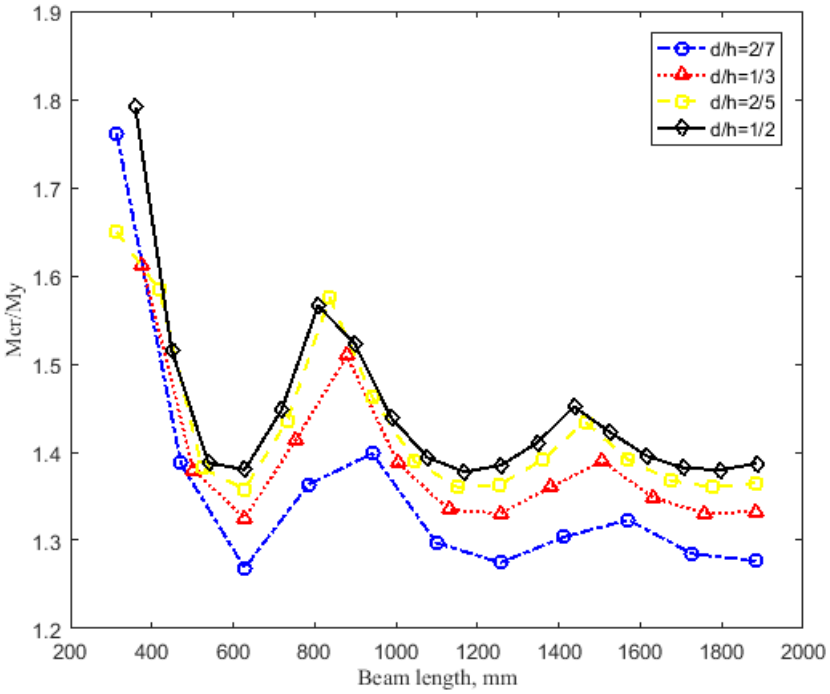

(b) Section 2 (h=200 mm, b=70 mm, c=20 mm, t=2.5 mm)

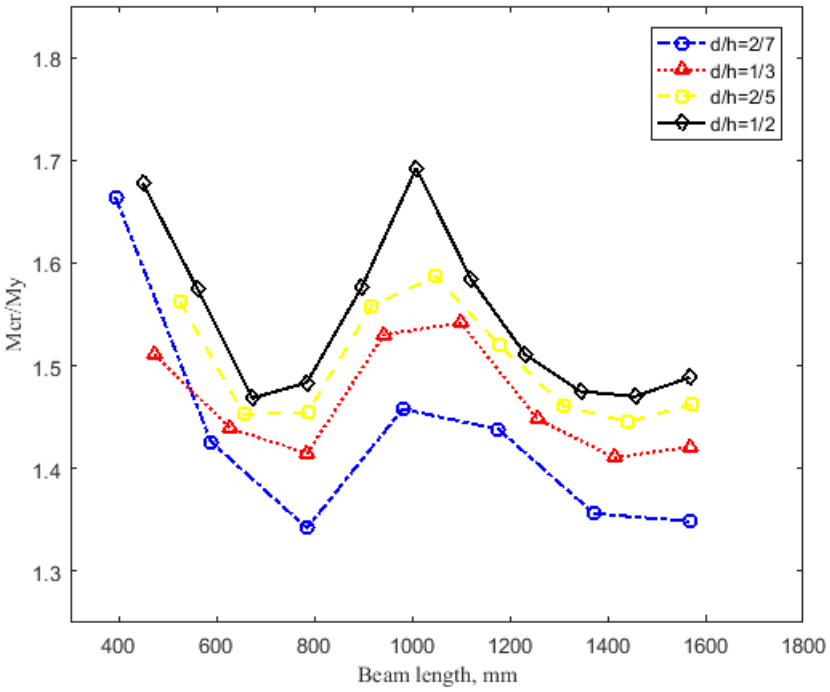

(c) Section 3 (h=250 mm, b=80 mm, c=25 mm, t=3 mm)

Fig. 6. Distortional buckling curves of PCFS channel-section beams (σ_y=390 MPa, M_y is the yield moment of CFS beams).

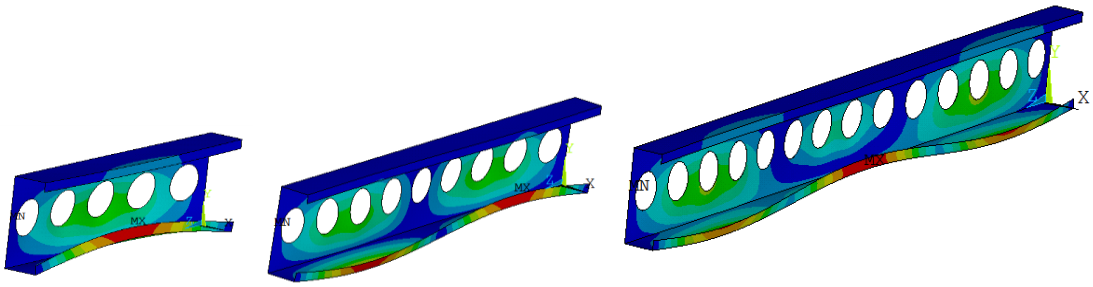

(a) Section 1 (h=150 mm, b=50 mm, c=15 mm, t=2 mm)

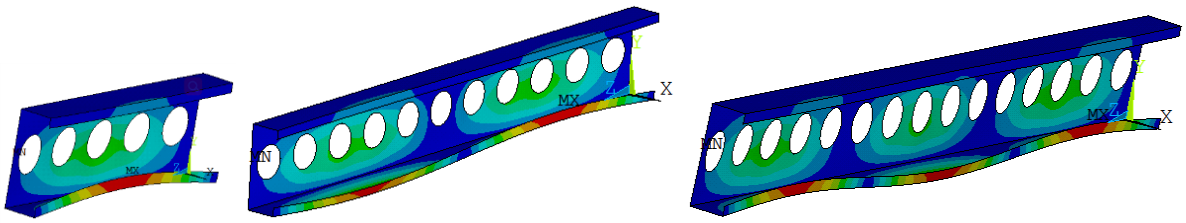

(b) Section 2 (h=200 mm, b=70 mm, c=20 mm, t=2.5 mm)

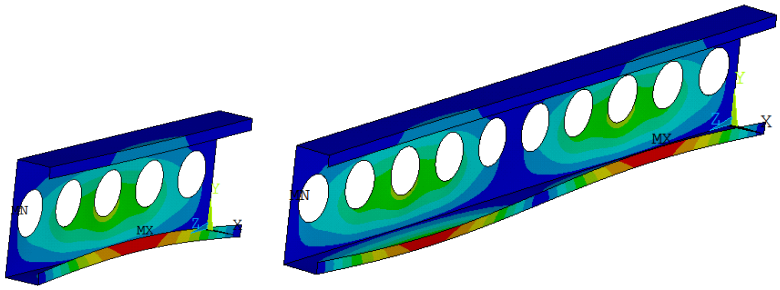

(c) Section 3 (h=250 mm, b=80 mm, c=25 mm, t=3 mm)

Fig. 7. Distortional buckling modes of PCFS channel-section beams.

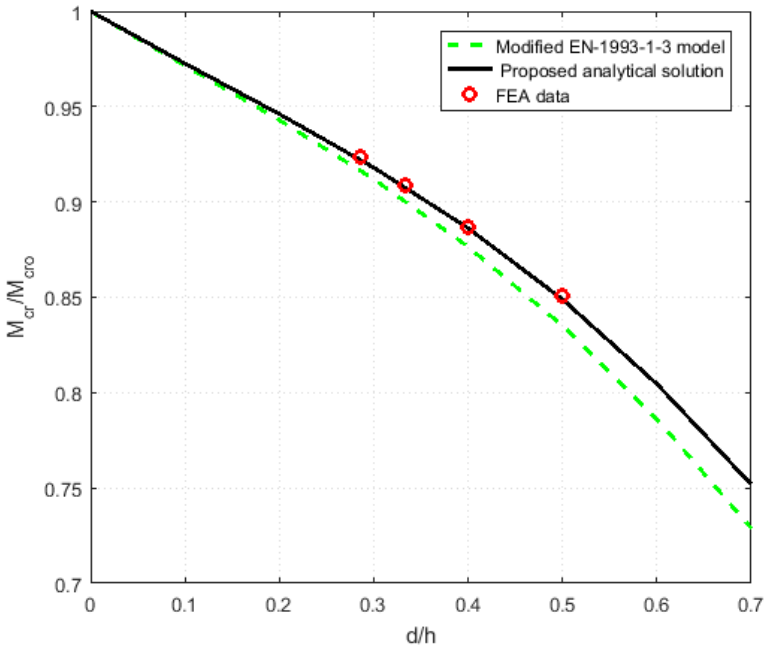

(a) Section 1 (h=150 mm, b=50 mm, c=15 mm, t=2 mm)

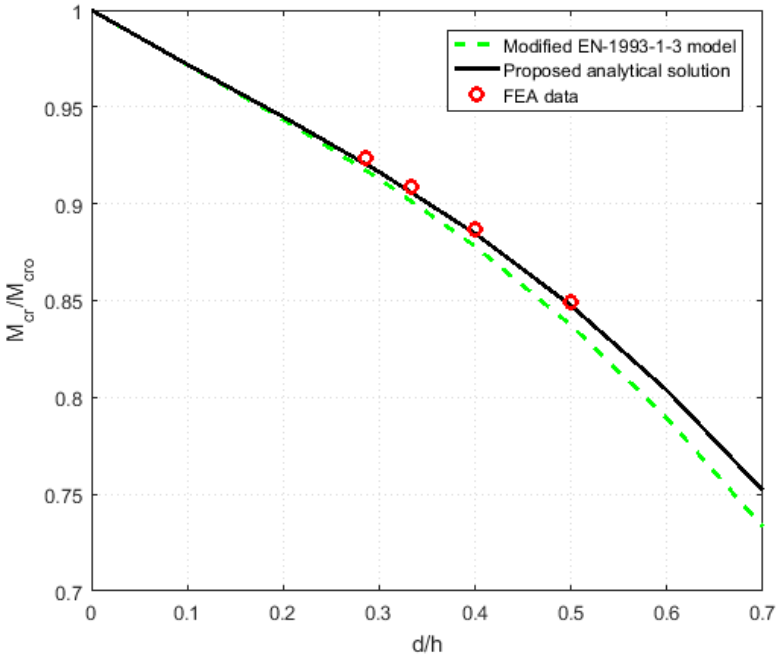

(b) Section 2 (h=200 mm, b=70 mm, c=20 mm, t=2.5 mm)

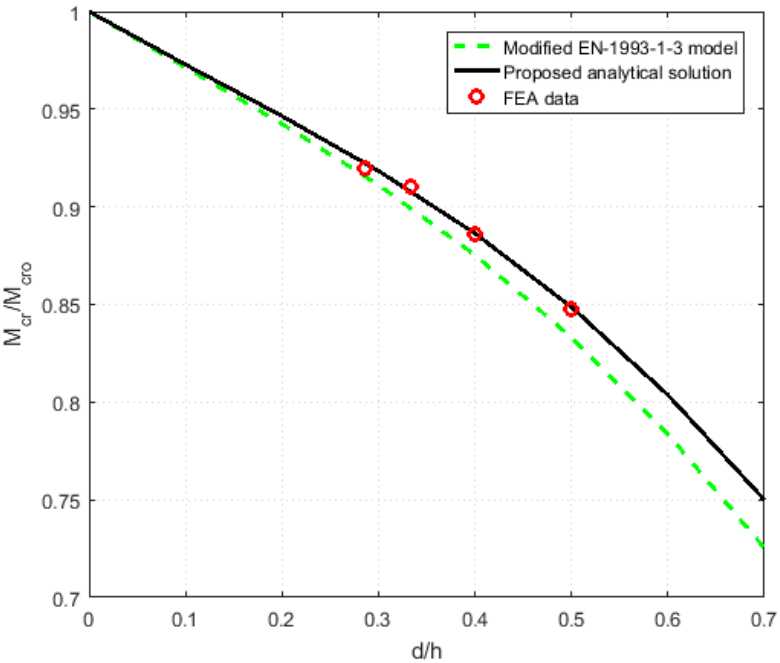

(c) Section 3 (h=250 mm, b=80 mm, c=25 mm, t=3 mm)

Fig. 8. Comparison of critical moments of distortional buckling of PCFS channel-section beams.